Blake J. Cochran,[1] Liming Hou,[1] Anil Paul Chirackal Manavalan,[1] Benjamin M. Moore,[2] Fatiha Tabet,[1] Afroza Sultana,[1] Luisa Cuesta Torres,[1] Shudi Tang,[1] Sudichhya Shrestha,[1] Praween Senanayake,[1] Mili Patel,[1] William J. Ryder,[1] Andre Bongers,[3] Marie Maraninchi,[4] Valerie C. Wasinger,[5] Marit Westerterp,[6] Alan R. Tall,[6] Philip J. Barter,[1,7] and Kerry-Anne Rye[1,7]

Impact of Perturbed Pancreatic β-Cell Cholesterol Homeostasis on Adipose Tissue and Skeletal Muscle Metabolism

Diabetes 2016;65:3610–3620 | DOI: 10.2337/db16-0668

Elevated pancreatic β-cell cholesterol levels impair insulin secretion and reduce plasma insulin levels. This study establishes that low plasma insulin levels have a detrimental effect on two major insulin target tissues: adipose tissue and skeletal muscle. Mice with increased β-cell cholesterol levels were generated by conditional deletion of the ATP-binding cassette transporters, ABCA1 and ABCG1, in β-cells (β-DKO mice). Insulin secretion was impaired in these mice under basal and high-glucose conditions, and glucose disposal was shifted from skeletal muscle to adipose tissue. The β-DKO mice also had increased body fat and adipose tissue macrophage content, elevated plasma interleukin-6 and MCP-1 levels, and decreased skeletal muscle mass. They were not, however, insulin resistant. The adipose tissue expansion and reduced skeletal muscle mass, but not the systemic inflammation or increased adipose tissue macrophage content, were reversed when plasma insulin levels were normalized by insulin supplementation. These studies identify a mechanism by which perturbation of β-cell cholesterol homeostasis and impaired insulin secretion increase adiposity, reduce skeletal muscle mass, and cause systemic inflammation. They further identify β-cell dysfunction as a potential therapeutic target in people at increased risk of developing type 2 diabetes.

The ATP-binding cassette transporters ABCA1 and ABCG1 regulate cell cholesterol homeostasis by exporting cellular cholesterol to extracellular acceptors (1–4). In the absence of ABCA1 and ABCG1, cell cholesterol levels increase (5,6) and cell function is impaired. In the case of pancreatic β-cells, increased cholesterol levels result in reduced insulin secretion (7). Loss-of-function mutations in the human *ABCA1* gene are also associated with cellular cholesterol accumulation, impaired glucose tolerance, and decreased insulin secretion but do not affect insulin sensitivity (8).

Increased adiposity, insulin resistance, impaired glucose tolerance, and/or impaired fasting glucose are all associated with a compensatory increase in β-cell mass and increased insulin secretion. This can eventually lead to β-cell failure, decreased insulin secretion, and development of type 2 diabetes mellitus (T2DM) (9,10). Decreased β-cell insulin secretion can precede the development of insulin resistance in individuals who are genetically predisposed to T2DM (11–14), in obese adolescents (15–19), in

[1]Lipid Research Group, School of Medical Sciences, Faculty of Medicine, University of New South Wales Australia, Sydney, Australia
[2]Division of Medicine, Royal Prince Alfred Hospital, Sydney, Australia
[3]Biological Resource Imaging Laboratory, Mark Wainwright Analytical Centre, University of New South Wales Australia, Sydney, Australia
[4]Aix-Marseille Université, UMR_S1062, UMR_A1260, Nutrition, Obésité et Risque Thrombotique, Marseille, France
[5]Bioanalytical Mass Spectrometry Facility, Mark Wainwright Analytical Centre, University of New South Wales Australia, Sydney, Australia
[6]Division of Molecular Medicine, Department of Medicine, Columbia University, New York, NY
[7]Faculty of Medicine, University of Sydney, Sydney, Australia

Corresponding author: Kerry-Anne Rye, k.rye@unsw.edu.au or karye@ozemail.com.au.

Received 30 May 2016 and accepted 23 September 2016.

This article contains Supplementary Data online at http://diabetes.diabetesjournals.org/lookup/suppl/doi:10.2337/db16-0668/-/DC1.

M.W. is currently affiliated with the Department of Pediatrics, Section on Molecular Genetics, University of Groningen, University Medical Center Groningen, Groningen, the Netherlands.

METABOLISM

people of Japanese descent (20–22), in Pima Indian populations (23) and in people with loss-of-function mutations in the *ABCA1* gene (24). These studies point to an impaired insulin response as an independent predictor of diabetes (25,26).

Previous studies have shown that mice with β-cell–specific deletion of ABCA1, alone (27,28) or together with global deletion of ABCG1 (6), have elevated β-cell cholesterol levels, reduced insulin secretion, and impaired glucose tolerance. However, because ABCA1 deletion in isolation leads to a compensatory elevation in ABCG1 expression (29) and ABCG1 knockout mice have very low adipose tissue mass and do not become glucose intolerant or insulin resistant when challenged with a high-fat diet (30), these studies have not provided insights into how β-cell dysfunction caused by perturbations in cholesterol homeostasis affects insulin target tissues, including adipose tissue and skeletal muscle. To better understand how dysregulated β-cell cholesterol homeostasis affects adipose tissue and skeletal muscle metabolism, we have generated mice with deletion of ABCA1 and ABCG1 only in β-cells (β-DKO mice).

RESEARCH DESIGN AND METHODS

Animal Studies

β-DKO mice were generated by crossing B6.Cg-Tg(Ins2-cre)25Mgn/J (The Jackson Laboratory) and *Abca1*fl/fl*Abcg1*fl/fl mice (31). All experiments were done in 16-week-old male mice, unless specified otherwise. The animals were maintained on a standard chow diet in a specific pathogen-free laboratory with a 12-h light/dark cycle. Food intake of 16-week-old mice was measured manually every 24 h over 3 consecutive days. Blood from the lateral tail vein was used for determining glucose levels (Accu-Chek Performa glucometer; Roche). Plasma interleukin (IL)-6 and MCP-1 levels were determined by ELISA (R&D Systems).

Quantification of Islet Cholesterol Levels

Pancreatic islets were isolated from 16-week-old mice as previously described (32), washed with PBS, and lysed with water. Total cholesterol levels in the cell lysates were quantified by high-performance liquid chromatography apparatus (33).

Glucose, Pyruvate, and Insulin Tolerance Tests

For glucose tolerance tests, mice were fasted for 5 h before an intraperitoneal injection of D-glucose (2 g/kg). For pyruvate tolerance tests, mice were fasted for 18 h before an intraperitoneal injection of sodium pyruvate (2 g/kg). For insulin tolerance tests, randomly fed mice received an intraperitoneal injection of 1 unit of human insulin per kilogram. Blood glucose levels (tail vein) were monitored at the indicated times.

Insulin Secretion Tests

Mice were fasted for 5 h before an intraperitoneal injection of D-glucose (3 g/kg) or arginine (1 g/kg). Blood was sampled from the lateral tail vein at 0, 5, 10, and 15 min. Plasma insulin concentrations were determined by ELISA (Merck Millipore).

Histology

Pancreata and epididymal adipose tissue were fixed with formalin and embedded in paraffin. Islets were visualized with an anti-insulin antibody (Cell Signaling) and an EnVision+ System-HRP kit (Dako). Adipose tissue sections were immunostained with hematoxylin and eosin for cell area determination or with an anti-F4/80 antibody for macrophage quantification (Abcam). Immunostained sections were quantified using the EnVision+ System-HRP kit. β-Cell mass was determined as previously described (34). Adipocyte area was determined using ImageJ software (National Institutes of Health).

EchoMRI

The percentage of body fat was determined using an EchoMRI-900 Body Composition Analyzer (EchoMRI, Biological Resources Imaging Laboratory, Mark Wainwright Analytical Centre, University of New South Wales, Sydney, Australia). The percentage body fat was calculated as ([body fat mass]/[body fat mass + lean mass]) × 100.

Glucose Uptake

Fasted mice were injected with [^{3}H]-2-deoxy-glucose (50 μCi/mouse) in 20% glucose (2 g/kg i.p.) and sacrificed after 2 h. Skeletal muscle and epididymal adipose tissue were harvested and frozen in liquid nitrogen until analysis. Tissues were homogenized in 0.5% (volume for volume [v/v]) perchloric acid and centrifuged at 2,000*g* for 20 min at 4°C. The supernatant was adjusted to pH 7.5 with KOH and split into two aliquots. Then, 2-deoxy-glucose phosphate was precipitated from one aliquot with 0.5 volume each of 0.3 mol/L BaOH and 0.3 mol/L $ZnSO_4$ and centrifuged at 16,000*g* for 5 min. Glucose uptake (as 2-deoxy-glucose phosphate) was quantified by liquid scintillation counting of the supernatant and the untreated aliquot and calculated as the difference between the two values (35).

Fatty Acid Synthase Activity Assay

Epididymal adipose tissue and liver samples (100 mg) were homogenized in ice-cold PBS containing 0.25 mol/L sucrose, 1 mmol/L dithiothreitol, 1 mmol/L EDTA-Na_2, and protease inhibitor (36). The samples were centrifuged at 20,000*g* for 10 min at 4°C, and then at 100,000*g* for 1 h at 4°C. The infranatant was mixed 1:1 (v/v) with 500 mmol/L phosphate buffer containing 0.5 mmol/L dithiothreitol (pH 7.4) and activated for 30 min at 37°C. The activated solution was added to two volumes of assay buffer (500 mmol/L potassium phosphate, 0.25 mmol/L NADPH, 0.1 mol/L EDTA-Na_2, and 1 mmol/L β-mercaptoethanol, pH 7), and incubated briefly. The reaction was started by adding substrate solution (10 μL of 5 mmol/L malonyl-CoA mixed 4:3 [v/v] with 5 mmol/L acetyl-CoA). The absorbance (340 nm) was measured continuously for 20 min. Fatty acid synthase activity was defined as 1 nmol NADPH consumed/min/mg protein using a molar (M) extinction coefficient of 6,220/M/cm.

Hepatic Glycogen and Plasma Lactate Levels

Livers were dissected, weighed, and snap frozen. Before analysis, the samples were placed on ice and homogenized in water. Glycogen levels were determined using a glycogen assay kit (Sigma-Aldrich). Plasma lactate levels were determined using a lactate assay kit (Abcam).

Western Blotting

Epididymal adipose tissue was isolated and homogenized with ice-cold radioimmune precipitation assay buffer. Cell lysates were electrophoresed on 4% homogeneous or 4–12% gradient SDS-PAGE gels for detection of fatty acid synthase and β-actin, respectively, and transferred to nitrocellulose membranes. The membranes were probed with monoclonal anti-rabbit fatty acid synthase (1:1,000; Cell Signaling) or anti-mouse β-actin (1:2,000; Abcam) primary antibodies and polyclonal sheep–anti-rabbit or sheep–anti-mouse horseradish peroxidase secondary antibodies (1:5,000; Abcam), developed with ECL Prime (GE Healthcare Life Sciences), and imaged using an ImageQuant LAS-4000 Mini (GE Healthcare Life Sciences). Band intensities were quantified using ImageJ.

Real-Time PCR

Total RNA was isolated from adipocytes (miRNeasy Mini kit; Qiagen) and reverse transcribed using 0.1 μg of RNA. Real-time PCR was performed with the MyiQ single-color real-time PCR detection system, using iQ SYBR Green Supermix (Bio-Rad) for relative mRNA quantification of the acetyl-CoA carboxylase-α (*Acaca)* and malonyl-CoA decarboxylase (*Mlycd*) genes. Values were normalized to GAPDH and expressed as $2^{-(\text{Ct[gene of interest]}-\text{Ct[GAPDH]})}$.

MRI

A circular polarized whole-body radiofrequency 50-mm volume quadrature coil was used for radiofrequency transmission and reception. For all MRI procedures, general anesthesia was induced with 4% isoflurane in oxygen (1 L/min) and maintained with 2–2.5% isoflurane. The animals were placed prone on the animal bed frame. The head was stabilized with a tooth-bar, and the liver region was centered within the scanner. A pressure-sensitive pad was used to monitor respiratory motion during imaging. The monitoring signal was used to trigger all imaging procedures to minimize image artifacts from abdominal motion. Animal body temperature was maintained at 36°C with a temperature-controlled circulating water warming blanket.

Images of the entire abdominal region were acquired in axial slice orientation using an optimized two-dimensional T1-weighted rapid acquisition with relaxation enhancement (TurboRARE) sequence. Parameters for the axial acquisitions were effective echo time = 8.5 ms, repetition time = 1,600 ms, field of view = 40 × 40 mm, acquisition matrix = 256 × 256 mm, in plane resolution = 156 × 156 μm, slice thickness = 1.0 mm, slice gap = 0.5 mm, number of slices = 40, resulting volume coverage = 59 mm, and 8 average, resulting in a total scan time of 10 min 20 s. All acquisitions were triggered "per phase step" on the breathing monitoring signal. To selectively highlight and identify fat localization, two identically positioned MRI volumes were acquired subsequently with and without fat presaturation but with otherwise identical imaging parameters. A fat suppression scheme using a Gaussian pulse with fat suppression bandwidth of 140 Hz, and 2 ms was used for the fat-saturated scan.

Mass Spectrometry

Mice were sacrificed by cervical dislocation, and gastrocnemius muscles were immediately dissected, weighed, snap frozen in liquid nitrogen, and stored at −80°C until processed. The samples (100 mg) were homogenized in ice-cold radioimmune precipitation assay buffer. Cell lysates were clarified by centrifugation at 10,000*g* for 10 min at 4°C. Proteins remaining in solution were precipitated by incubation with four volumes of ice-cold acetone and collected by centrifugation at 13,000*g* for 10 min at 4°C. The cell pellets were resuspended in 50 mmol/L ammonium bicarbonate (pH 8.0), and protein concentrations were quantified by bicinchoninic acid assay (Life Technologies).

Whole-cell protein extracts (100 μg) were adjusted to 20 μL with 50 mmol/L NH_4HCO_3 (pH 8). Trypsin (Promega) was added (final enzyme-to-protein ratio was 1:100 [w/w]) and incubated overnight at 37°C. The reaction was stopped by adjustment to ~pH 3 with neat formic acid, and the samples were dried (vacuum centrifuge) and stored at −20°C until analyzed. The resulting peptides were purified using C18 StageTips (Thermo Fisher Scientific).

Peptides were reconstituted in 10 μL of 0.1% formic acid and separated by nano-LC using an Ultimate3000 high-performance liquid chromatography apparatus and autosampler (Dionex). Samples (0.2 μL, ~2 μg in total) were loaded onto a micro C18 precolumn (500 μm–2 mm; Michrom Bioresources) with Buffer C (97.95% H_2O, 1.95% CH_3CN, 0.1% trifluoroacetic acid) at a flow rate of 10 μL/min. After a 4-min wash, the precolumn was switched (Valco 10-port valve; Dionex) into line with a fritless nano column (75 μm internal diameter, 12 cm) containing reverse-phase C18 media (3 μm, 200 Å Magic, Michrom Bioresources). The peptides were eluted using a linear gradient of Buffer C to Buffer D (97.95% CH_3CN, 1.95% H_2O, 0.1% formic acid) at 250 nL/min over 1 h. High voltage (2,000 V) was applied to a low volume tee (Upchurch Scientific) and the column tip positioned 0.5 cm from the heated capillary (T = 280°C) of an Orbitrap Velos (Thermo Electron, Thermo Fisher Scientific) mass spectrometer. Positive ions were generated by electrospray, and the Orbitrap operated in data-dependent acquisition mode. A survey scan mass (m)-to-charge (z) ratio of 350–1,750 was acquired (resolution = 30,000 at an m-to-z ratio of 400, with an accumulation target value of 1,000,000 ions) with lock mass enabled. Up to the 10 most abundant ions (45,000 counts) with charge states +2 to +4 were sequentially isolated and fragmented within the linear ion trap using collisionally induced dissociation with an activation q = 0.25 and activation time of 30 ms at a target value of 30,000 ions. The m-to-z ratio selected for tandem mass spectrometry (MS/MS) was dynamically excluded for 30 s. MS peak intensities were analyzed using Progenesis LC–MS 4 data analysis software (Nonlinear Dynamics). Ion intensity maps from each run were aligned to a reference sample. Ion feature matching was achieved by aligning consistent ion m-to-z ratio and retention times.

The peptide intensities were normalized against total intensity (sample specific log-scale abundance ratio-scaling factor) and compared by ANOVA. Type I errors were controlled for by false discovery rate with *q* value for significance set at 0.01 (37). MS/MS spectra were searched against the National Center for Biotechnology Information nonredundant protein database using MASCOT (Matrix Science). Parent and fragment ions were searched with tolerances of 6 ppm and 0.6 Da, respectively, with mouse proteins selected and "no-enzyme" specified.

Insulin Supplementation

Mini osmotic pumps (Model 1004, Alzet) loaded with 33.34 units/mL Humulin R (corresponding to a dose of 0.1 units/day; Eli Lily) or an equivalent volume of PBS were inserted subcutaneously between the shoulder blades of anesthetized 12-week-old β-DKO mice (38). After sacrifice at 16 weeks of age, the percentage of body fat was determined by EchoMRI. Adipocyte area and adipose tissue macrophage content were quantified using ImageJ (39).

Statistical Analysis

Results are presented as mean ± SD. Significant differences between experimental groups were determined using an unpaired, two-tailed Student *t* test or one-way ANOVA with Tukey posttest, as appropriate. $P < 0.05$ was considered as significant.

RESULTS

Conditional β-Cell Deletion of ABCA1 and ABCG1 Increases Cellular Cholesterol Levels and Glucose Intolerance and Impairs Insulin Secretion

β-DKO mice were generated by crossing B6.Cg-Tg(Ins2-Cre) 25Mgn/J (Ins2Cre) and *Abca1*fl/fl*Abcg1*fl/fl mice (31). ABCA1 and ABCG1 protein levels in the β-DKO mice islets were decreased by 82.0 ± 5.1% and 84.4 ± 1.2%, respectively, relative to *Abca1*fl/fl*Abcg1*fl/fl mice (Fig. 1*A* and *B*).

The body weight (Fig. 2*A*) and food intake (Fig. 2*B*) of the β-DKO mice were comparable to that of the *Abca1*fl/fl*Abcg1*fl/fl mice and Ins2Cre mice. Although there were no differences in fed or fasting blood glucose levels in 6-, 12-, or 16-week-old β-DKO, *Abca1*fl/fl*Abcg1*fl/fl, and Ins2Cre mice (Fig. 2*C*), values for the β-DKO mice were more variable, especially under fasting conditions. Fed and fasting plasma insulin levels were both significantly decreased in 6-, 12-, and 16-week-old β-DKO mice compared with *Abca1*fl/fl*Abcg1*fl/fl littermates ($P < 0.001$ for all) (Fig. 2*D*).

Intraperitoneal glucose tolerance tests revealed that the β-DKO mice were glucose intolerant relative to *Abca1*fl/fl*Abcg1*fl/fl and Ins2Cre mice (incremental area under the curve: 589.3 ± 203.8, 608.5 ± 187.3, and 1,657.0 ± 272.7 for *Abca1*fl/fl*Abcg1*fl/fl, Ins2Cre, and β-DKO mice, respectively; $P < 0.001$ for β-DKO vs. *Abca1*fl/fl*Abcg1*fl/fl mice) (Fig. 2*E* and *F*). Pyruvate tolerance tests indicated normal gluconeogenesis in β-DKO mice (Fig. 2*G*). Liver mass and glycogen levels were also comparable in the β-DKO and *Abca1*fl/fl*Abcg1*fl/fl mice (Supplementary Table 1). β-DKO mice also had normal insulin sensitivity (Fig. 2*H*). Fasting insulin levels were significantly lower in β-DKO mice (0.67 ± 0.19 ng/mL) compared with *Abca1*fl/fl*Abcg1*fl/fl mice (1.03 ± 0.18 ng/mL, $P < 0.001$). The first phase of insulin secretion in response to both a glucose (Fig. 2*I*) and arginine (Fig. 2*J*) challenge was lost in the β-DKO mice.

Islet morphology and β-cell mass were normal in the β-DKO mice (Fig. 2*K* and *L*) despite islet cholesterol levels being elevated to 19.2 ± 1.9 mg/mg protein compared with 8.7 ± 1.0 mg/mg protein in *Abca1*fl/fl*Abcg1*fl/fl mice ($P < 0.001$).

β-DKO Mice Have Increased Adiposity and Decreased Muscle Mass Relative to Littermate Controls

The 16-week-old, chow-fed β-DKO mice had strikingly increased visceral and subcutaneous fat deposition relative to *Abca1*fl/fl*Abcg1*fl/fl mice (Fig. 3*A*). This was confirmed by MRI (Fig. 3*B*), which showed that 16-week-old β-DKO mice had 16.2 ± 1.3% body fat compared with 10.5 ± 0.9% for *Abca1*fl/fl*Abcg1*fl/fl mice ($P < 0.001$) (Fig. 3*C*). Because the body weights of the β-DKO and *Abca1*fl/fl*Abcg1*fl/fl mice were comparable (Fig. 2*A*), this suggested that the adipose tissue expansion may have been at the expense of a reduction in skeletal muscle mass.

This was confirmed by establishing that hind limb gastrocnemius muscle mass was decreased to 87.0 ± 11.4 mg in the β-DKO mice compared with 123.8 ± 17.6 mg in *Abca1*fl/fl*Abcg1*fl/fl mice ($P < 0.005$) (Fig. 3*D* and *E*). The increased percentage of body fat in the β-DKO mice was caused by adipocyte hypertrophy, with an average adipocyte area in the β-DKO mice of 4,445.7 ± 514.3 μm^2 compared with 3,386 ± 439.7 μm^2 for *Abca1*fl/fl*Abcg1*fl/fl mice ($P < 0.001$) (Fig. 3*F*).

β-DKO Mice Have Systemic Inflammation and Increased Adipose Tissue Macrophage Content

Macrophage infiltration was apparent in the β-DKO mouse adipose tissue, with 1.71 ± 1.056% of the cells staining positive for F4/80+ compared with 0.22 ± 0.38% in the

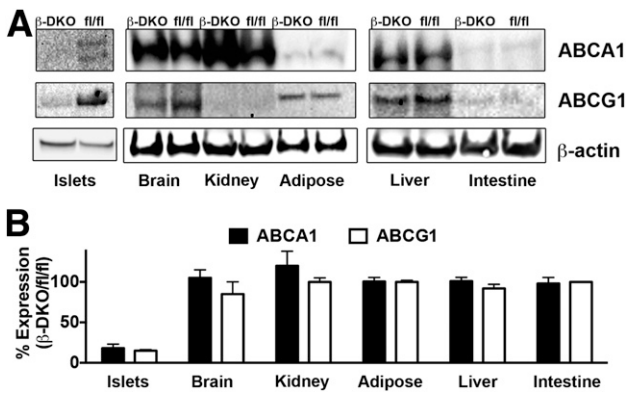

Figure 1—Conditional deletion of ABCA1 and ABCG1 in β-DKO mice. *A*: Tissue homogenates from β-DKO and *Abca1*fl/fl*Abcg1*fl/fl mice were subjected to SDS-PAGE and immunoblotted for ABCA1, ABCG1, and β-actin. *B*: Quantification of blots from *A*. Results represent the mean ± SD of three independent experiments.

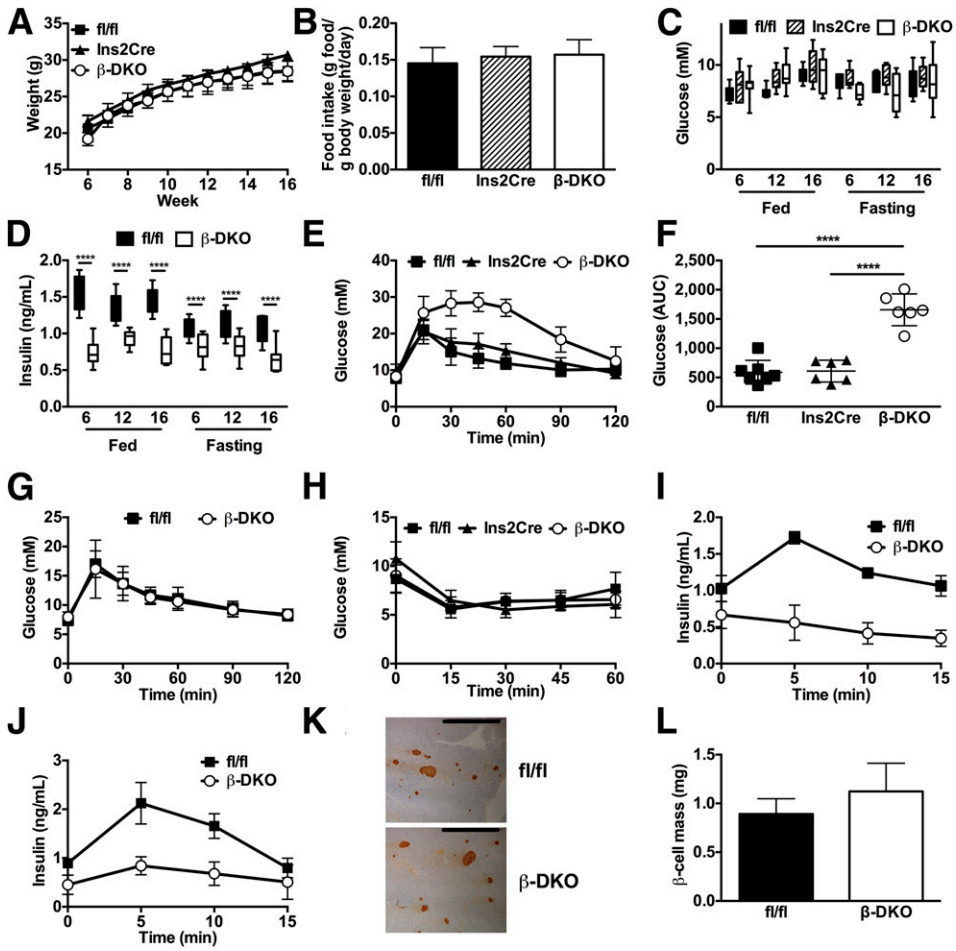

Figure 2—Glucose tolerance and insulin secretion are impaired in β-DKO mice. *A*: Body weight of 6- to 16-week-old *Abca1*fl/fl*Abcg1*fl/fl mice, Ins2Cre mice, and β-DKO mice (n = 6/group). *B*: Daily food intake of 16-week-old *Abca1*fl/fl*Abcg1*fl/fl mice, Ins2Cre mice, and β-DKO mice (n = 6/group). Fed and 5-h fasted blood glucose (*C*) and insulin (*D*) levels in 6-, 12-, and 16-week-old *Abca1*fl/fl*Abcg1*fl/fl mice, Ins2Cre mice, and β-DKO mice (n = 8–10/group). Blood glucose levels (*E*) and incremental area under curve (AUC) data (*F*) during an intraperitoneal glucose tolerance test (glucose: 2 g/kg) in 5-h fasted, 16-week-old *Abca1*fl/fl*Abcg1*fl/fl mice, Ins2Cre mice, and β-DKO mice (n = 6–8/group). *G*: Blood glucose levels during an intraperitoneal pyruvate tolerance test (sodium pyruvate: 2 g/kg) in 18-h fasted, 16-week-old *Abca1*fl/fl*Abcg1*fl/fl mice and β-DKO mice (n = 6/group). *H*: Blood glucose levels during an intraperitoneal insulin tolerance test (insulin: 1 unit/kg; n = 7/group) in 16-week-old *Abca1*fl/fl*Abcg1*fl/fl mice, Ins2Cre mice, and β-DKO mice. Plasma insulin levels during a glucose (*I*) and arginine (*J*) challenge in *Abca1*fl/fl*Abcg1*fl/fl mice and β-DKO mice. The mice were fasted for 5 h before intraperitoneal administration of 3 g/kg glucose or 1 g/kg arginine. Plasma insulin levels were measured by ELISA (n = 7/group). *K*: Representative pancreas sections from *Abca1*fl/fl*Abcg1*fl/fl mice and β-DKO mice immunostained for insulin. Scale bars = 1 mm. *L*: Quantification of β-cell mass in *Abca1*fl/fl*Abcg1*fl/fl mice and β-DKO mice. Values represent mean ± SD. In the box-and-whisker plots, line in box represents median quartile; whiskers represent minimum-maximum values; box borders represent lower and upper quartiles. ****$P < 0.001$.

*Abca1*fl/fl*Abcg1*fl/fl mice ($P < 0.01$) (Fig. 4*A* and *B*). Plasma IL-6 (Fig. 4*C*) and MCP-1 (Fig. 4*D*) levels were also increased in the β-DKO mice (11.0 ± 3.2 and 57.1 ± 4.0 pg/mL, respectively) relative to *Abca1*fl/fl*Abcg1*fl/fl mice (2.8 ± 0.2 and 11.4 ± 5.6 pg/mL, respectively; $P < 0.005$ for IL-6 and $P < 0.001$ for MCP-1).

Glucose Uptake Is Shifted From Skeletal Muscle to Adipose Tissue in β-DKO Mice

We next asked whether the increased adiposity and decreased muscle mass in the β-DKO mice could be explained by the limited availability of insulin (Fig. 2*D*, *I*, and *J*) causing glucose disposal to be redirected from skeletal muscle to adipose tissue. This was found to be the case, with the uptake of [^{3}H]-2-deoxyglucose by skeletal muscle reduced to 176.4 ± 23.1 nmol/g/min in the β-DKO mice compared with 241.1 ± 25.6 nmol/g/min in *Abca1*fl/fl*Abcg1*fl/fl mice ($P < 0.01$) (Fig. 5*A*). [^{3}H]-2-deoxyglucose uptake into epididymal adipose tissue was concomitantly increased from 24.5 ± 5.4 nmol/g/min in *Abca1*fl/fl*Abcg1*fl/fl mice to 36.7 ± 8.9 nmol/g/min in β-DKO mice ($P < 0.05$) (Fig. 5*B*).

The underlying cause of the preferential disposal of glucose in adipose tissue in β-DKO mice was also investigated. Hepatic fatty acid synthase activity was comparable in the β-DKO and control mice (Fig. 5*C*). Fatty acid synthase activity was significantly elevated in β-DKO mouse adipose tissue (7.77 ± 0.50 nmol/min/mg compared with 5.10 ± 1.70 nmol/min/mg for *Abca1*fl/fl*Abcg1*fl/fl mice

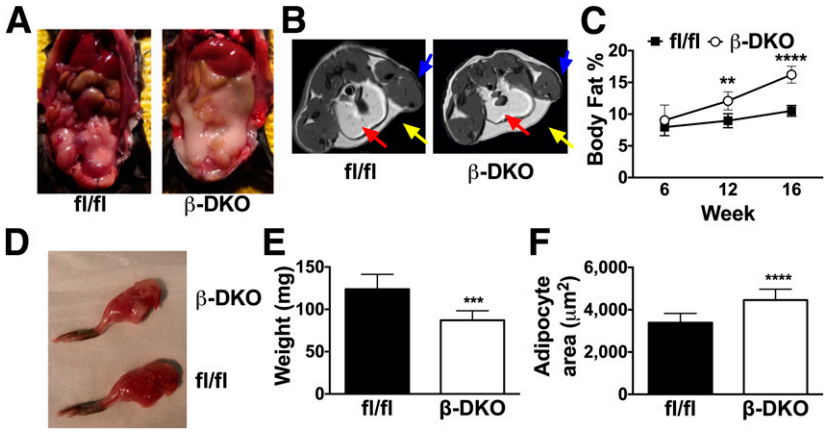

Figure 3—Adipose tissue mass is increased and skeletal muscle mass is decreased in β-DKO mice. *A*: Representative images of visceral fat in 16-week-old *Abca1*fl/fl*Abcg1*fl/fl mice and β-DKO mice. *B*: Representative transverse section of MRI displays the differences in visceral (red arrow) and subcutaneous (yellow arrow) adipose tissue and hind limb muscle (blue arrow) size in 16-week-old *Abca1*fl/fl*Abcg1*fl/fl mice and β-DKO mice. *C*: Body fat percentage by EchoMRI in 6-, 12-, and 16-week-old *Abca1*fl/fl*Abcg1*fl/fl mice and β-DKO mice (n = 6/group). *D*: Representative image of skeletal muscle in dissected hind limb in 16-week-old β-DKO mice and *Abca1*fl/fl*Abcg1*fl/fl mice. *E*: Weight of isolated gastrocnemius muscle in 16-week-old *Abca1*fl/fl*Abcg1*fl/fl mice and β-DKO mice (n = 8/group). *F*: Quantification of adipocyte size in 16-week-old *Abca1*fl/fl*Abcg1*fl/fl mice and β-DKO mice (n = 8/group, 10 sections/animal). Values represent mean ± SD. ***P < 0.005; ****P < 0.001.

and 3.84 ± 0.31 nmol/min/mg protein for Ins2Cre mice; P < 0.05 β-DKO vs. *Abca1*fl/fl*Abcg1*fl/fl, and P < 0.01 β-DKO vs. Ins2Cre) (Fig. 5*D*) Despite the increased adipose tissue fatty acid synthase activity, adipocyte fatty acid synthase protein levels were decreased in the β-DKO mice relative to the *Abca1*fl/fl*Abcg1*fl/fl mice (Fig. 5*E* and *F*).

Protein levels of the fatty acid synthase substrate, malonyl-CoA, and mRNA levels of acetyl-CoA carboxylase-α (ACACA), the enzyme that converts acetyl-CoA to malonyl-CoA and malonyl-CoA decarboxylase (MLYCD), which converts malonyl-CoA back into acetyl-CoA, were also determined. Adipocyte malonyl-CoA levels were decreased in β-DKO mice relative to *Abca1*fl/fl*Abcg1*fl/fl mice (2.73 ± 0.943 vs 8.03 ± 2.74 ng/mg protein, respectively; P < 0.01) (Fig. 5*G*) Adipocyte MLYCD mRNA levels were, by contrast, increased in the β-DKO mice (Fig. 5*H*). There was a trend toward reduced ACACA mRNA levels in the β-DKO mice, but this did not reach statistical significance (Fig. 5*I*).

The effect of decreased glucose uptake on skeletal muscle metabolism was investigated by MS. Significant changes were observed in the expression of 53 proteins (Supplementary Table 2 and Supplementary Fig. 1). Ingenuity Pathway analysis of the differentially expressed proteins revealed significant changes in a number of skeletal muscle enzymes involved in glycolysis, gluconeogenesis, and amino acid metabolism in β-DKO mice relative to *Abca1*fl/fl*Abcg1*fl/fl mice (Table 1).

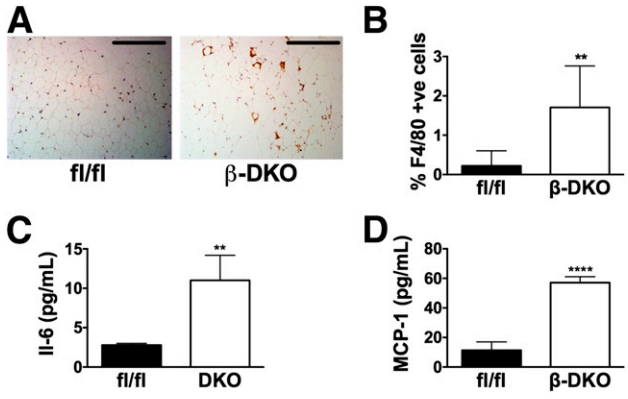

Figure 4—β-DKO mice have increased adipose tissue macrophage content and systemic inflammation. *A*: Representative histology of F4/80+ staining in adipose tissue from *Abca1*fl/fl*Abcg1*fl/fl mice and β-DKO mice. Scale bars = 200 μm. *B*: Quantification of F4/80 staining from *A* (n = 8/group, 10 sections/animal). Plasma IL-6 (*C*) and MCP-1 (*D*) levels in 16-week-old *Abca1*fl/fl*Abcg1*fl/fl mice and β-DKO mice (n = 6/group). Values represent mean ± SD. **P < 0.01; ****P < 0.001.

Insulin Supplementation Ablates Adipose Tissue Expansion in β-DKO Mice

To ascertain whether the increased adiposity in the 16-week-old β-DKO mice was caused by their suboptimal plasma insulin levels (Fig. 2*D*, *I*, and *J*), osmotic pumps were loaded with insulin (Humulin R, 0.1 units/day) or PBS (control) and implanted in two groups of 12-week-old β-DKO mice (38). The animals were sacrificed 4 weeks postpump implantation. No difference in body weight was observed between the insulin-supplemented and PBS-supplemented β-DKO mice (Fig. 6*A*). At 1 week postpump implantation, plasma insulin levels in the insulin-supplemented mice were 1.0 ± 0.2 ng/mL compared with 0.5 ± 0.1 ng/mL in the PBS-treated mice (P < 0.005) (Fig. 6*B*). Insulin levels in the insulin-supplemented mice remained constant and comparable to the insulin levels in

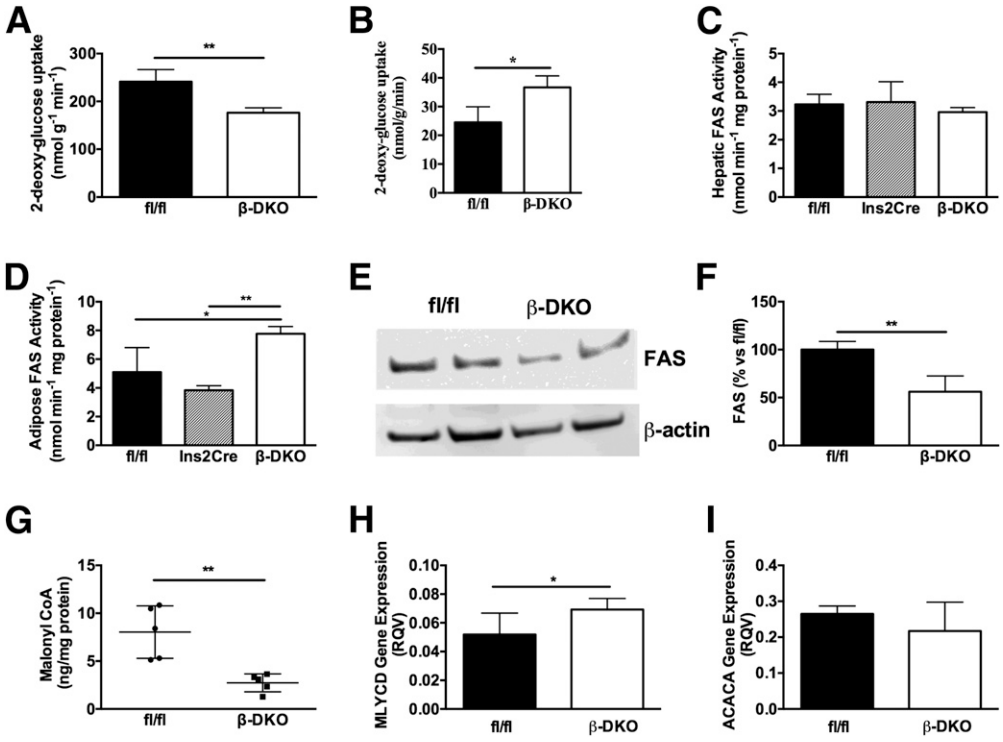

Figure 5—Impaired insulin secretion shifts glucose disposal from skeletal muscle to adipose tissue in β-DKO mice. Uptake of [^{3}H]-2-deoxyglucose in muscle (*A*) and epididymal adipose tissue (*B*) in *Abca1*fl/fl*Abcg1*fl/fl mice and β-DKO mice (n = 6/group). Fatty acid synthase (FAS) activity in isolated liver (*C*) and epididymal adipose tissue (*D*) in *Abca1*fl/fl*Abcg1*fl/fl mice, Ins2Cre mice, and β-DKO mice (n = 6/group). FAS expression in *Abca1*fl/fl*Abcg1*fl/fl and β-DKO mouse epididymal adipose tissue assessed by Western blotting (*E*) and quantification of FAS expression (*F*). *G*: Isolated adipocyte levels of malonyl-CoA levels were determined by ELISA. *Mlycd* (*H*) and *Acaca* (*I*) mRNA levels were determined by real-time PCR (n = 5/group). RQV, relative quantification value. Values represent mean ± SD. *$P < 0.05$; **$P < 0.01$.

the *Abca1*fl/fl*Abcg1*fl/fl mice until sacrifice at 16 weeks of age. Insulin supplementation did not affect β-DKO mice blood glucose levels (Fig. 6*C*), but it completely ablated body fat accumulation. The insulin-supplemented β-DKO mice had 13.4 ± 2.3% body fat at 16 weeks of age compared with 18.0 ± 2.1% body fat for the PBS-treated β-DKO mice ($P < 0.05$) (Fig. 6*D*). Insulin supplementation also increased β-DKO mouse gastrocnemius muscle weight to 105.0 ± 8.9 mg compared with 85.8 ± 8.5 mg for PBS-treated β-DKO mice ($P < 0.01$) (Fig. 6*E*). Moreover, adipocyte area decreased from 4,380 ± 342 μm^2 in the PBS-treated β-DKO mice to 3,923 ± 213 μm^2 in the insulin-supplemented β-DKO mice ($P < 0.01$) (Fig. 6*F*). Insulin supplementation did not change β-cell mass (Fig. 6*G*), adipose tissue macrophage content (Fig. 6*H*), or plasma IL-6 (Fig. 6*I*) and MCP-1 levels (Fig. 6*J*). Although insulin tolerance was not altered in the insulin-supplemented mice (Supplementary Fig. 2*A*), glucose tolerance was significantly improved, most likely as a result of increased skeletal muscle mass (Supplementary Fig. 2*B*).

DISCUSSION

This study establishes that the increased β-cell cholesterol levels in β-DKO mice reduces insulin secretion in response

Table 1—Altered metabolic pathways in isolated gastrocnemius muscle from β-DKO mice

Pathway	Upregulated	Downregulated	*P* value
Glycolysis	BPGM, FBP2, PGAM2, PGK1, PKM	GAPDH, GPI	2.97E-13
Gluconeogenesis	BPGM, FBP2, PGAM2, PGK1	GAPDH, GPI	3.50E-11
Rapoport-Luebering glycolytic shunt	BPGM, PGAM2		4.61E-05
Glutaryl-CoA degradation	ACoAAT, HSD17B10		5.00E-04
Isoleucine degradation	ACoAAT, HSD17B10		7.91E-04

Gastrocnemius muscle was obtained from 16-week-old β-DKO mice and *Abca1*fl/fl/*Abcg1*fl/fl mice at the time of sacrifice. The samples were homogenized, and proteins were precipitated with acetone and digested with trypsin, as described in RESEARCH DESIGN AND METHODS. The resulting peptides were purified and analyzed by MS and Ingenuity Pathway Analysis.

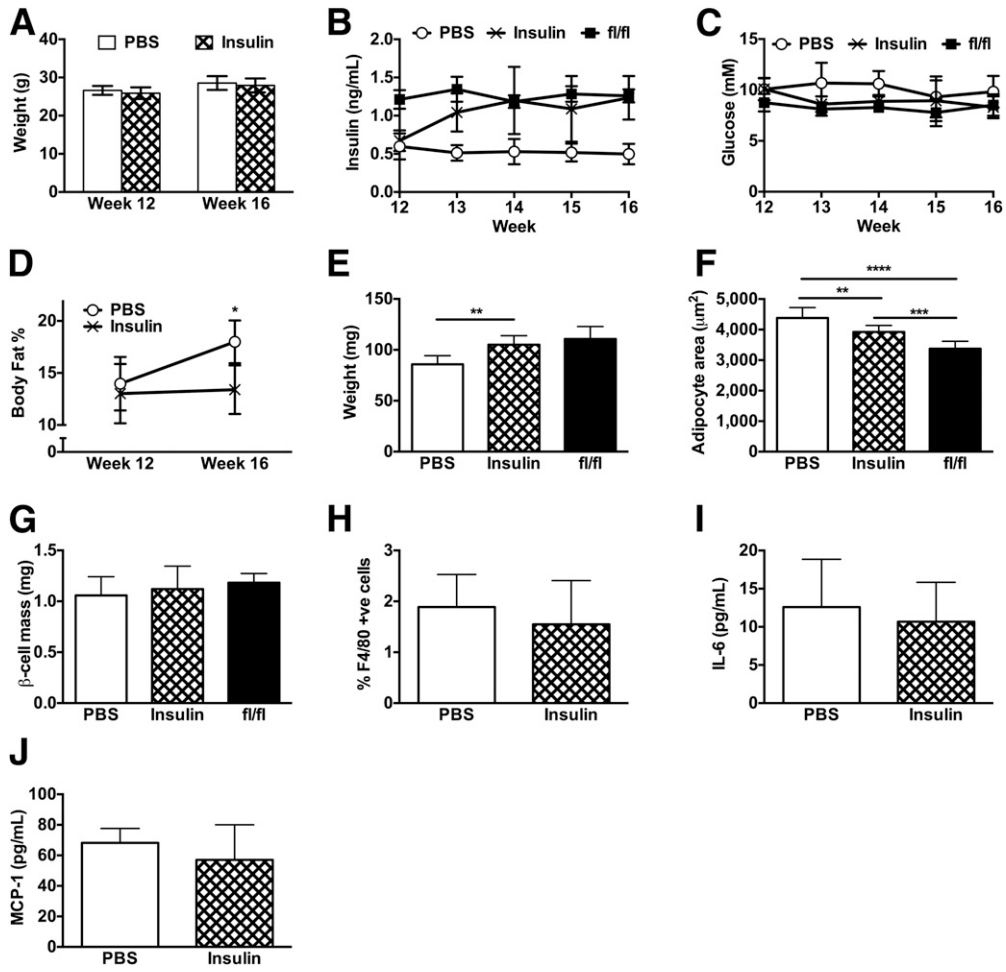

Figure 6—Insulin supplementation inhibits adipose tissue expansion but does not reduce inflammation in β-DKO mice. *A*: Body weight of β-DKO mice immediately before pump implantation at 12 weeks of age and at 16 weeks of age, after 4 weeks of PBS or insulin supplementation. Fed plasma insulin levels (*B*) and blood glucose levels (*C*) in PBS- and insulin-supplemented β-DKO mice and *Abca1*fl/fl*Abcg1*fl/fl mice. *D*: Percentage of body fat in PBS- and insulin-supplemented β-DKO mice. *E*: Gastrocnemius muscle weight in 16-week-old PBS- and insulin-supplemented β-DKO mice and *Abca1*fl/fl*Abcg1*fl/fl mice. Adipocyte size (*F*), β-cell mass (*G*), and adipose tissue macrophage content (*H*) in PBS- and insulin-supplemented β-DKO mice and *Abca1*fl/fl*Abcg1*fl/fl mice. Plasma IL-6 (*I*) and MCP-1 (*J*) levels in PBS- and insulin-supplemented β-DKO mice. Values represent mean ± SD (n = 6/group for all). *$P < 0.05$; **$P < 0.01$; ***$P < 0.005$; ****$P < 0.001$.

to glucose and leads to glucose intolerance but does not cause insulin resistance. It also shifts glucose uptake from skeletal muscle to adipose tissue in a process that is accompanied by adipocyte hyperplasia, infiltration of macrophages into adipose tissue, and systemic inflammation.

Cholesterol is known to be toxic to β-cells (40), but the extent of β-cell cholesterol accumulation in β-DKO mice was clearly below the threshold that causes cell death. This is in contrast to what has been reported for mice transgenic for SREBP-1c, where increased β-cell cholesterol levels decreased islet size and number (41). Furthermore, islet hypertrophy was not evident in the β-DKO mice, which is consistent with the absence of insulin resistance (42).

Conditional β-cell deletion of ABCA1 and ABCG1 did not affect body weight or gross locomotion (42) but did increase body fat and decrease muscle mass relative to littermate controls. This is in contrast to reports of mice with β-cell–specific deletion of ABCA1, in isolation (28) or on a global ABCG1 knockout background (6), where body composition did not change. This discrepancy is most likely caused by a compensatory rise in ABCG1 expression in mice with β-cell–specific deletion of ABCA1 only (29), and ABCG1 deletion protecting animals with β-cell–specific deletion of ABCA1 from obesity (30).

The absence of hyperglycemia in β-DKO mice is consistent with other reports of normal blood glucose levels in mice with low plasma insulin levels (43–45). In the case of β-DKO mice, this phenotype is likely a result of normal insulin sensitivity combined with plasma insulin levels that are still sufficient to normalize blood glucose levels. However, increased variability in fasting blood glucose levels was observed in the β-DKO mice. This suggests that regulation of glucose homeostasis in these animals is impaired, which is consistent with the altered levels of skeletal muscle proteins involved in glycolysis and gluconeogenesis.

Furthermore, because type 10,17 β-hydroxysteroid dehydrogenase (HSD17B10) and acetyl-CoA acetyltransferase (ACoAAT), which, respectively, catalyze the final steps in the conversion of isoleucine and methylated fatty acids to acetyl-CoA (46), were both upregulated in β-DKO mouse gastrocnemius muscle, it follows that these animals must use substrates other than glucose for energy production in skeletal muscle. In addition, the comparable glucose levels in β-DKO and control mice, despite significant differences in insulin levels, suggests that noninsulin-dependent glucose uptake is enhanced in β-DKO mouse skeletal muscle. Although no difference in AMPK activation between the β-DKO and control mice was observed (data not shown), it is possible that other pathways, such as Ca^{2+}/calmodulin signaling, are involved.

A key finding from this study is that insulin insufficiency shifted glucose disposal from skeletal muscle to adipose tissue in β-DKO mice. This is probably related to the fact that approximately twice as much insulin is required to mediate the same amount of glucose uptake and metabolism in skeletal muscle than in adipose tissue (47). This suggests that when insulin availability is compromised, glucose uptake and metabolism in skeletal muscle are affected more severely than in adipose tissue. It is also consistent with altered skeletal muscle metabolism in the β-DKO mice and is in agreement with the observed increase in fatty acid synthase activity in adipose tissue. The increased fatty acid synthase activity in β-DKO mouse adipose tissue may be a reflection of enhanced enzyme dimerization in the hypertrophied adipocytes (48). The reduced adipocyte fatty acid synthase protein levels in the β-DKO mice, by contrast, are most likely a downstream consequence of insulin insufficiency, because insulin is required for the induction of fatty acid synthase gene transcription (49). Despite previous reports that malonyl-CoA levels rise during fatty acid synthesis (50), the level was decreased in adipocytes from β-DKO mice. This may be caused by increased incorporation of malonyl-CoA into fatty acids and increased MLYCD-mediated conversion of malonyl-CoA to acetyl-CoA. Interestingly, increased adiposity was not observed in insulin-insufficient, chow-fed $Ins1^{+/-}Ins2^{-/-}$ mice (45), possibly as a result of increased energy expenditure and expression of uncoupling protein 1 in white adipose tissue.

Although inflammation is usually associated with increased circulating insulin levels and insulin resistance (51), the results in this study provide compelling evidence that inflammation can also be driven by adipose tissue expansion in the absence of insulin resistance. It is possible that insulin supplementation did not reduce adipose tissue inflammation in β-DKO mice because chronically elevating plasma insulin levels in these animals may enhance adipose tissue lipolysis (52), which increases macrophage recruitment (53). Moreover, the absence of insulin resistance in β-DKO mice with adipocyte hypertrophy and adipose tissue inflammation is in line with reports of insulin resistance being driven by lipid accumulation in nonadipose tissues (54,55).

In conclusion, this study shows that elevated β-cell cholesterol levels lead to β-cell dysfunction, increased adiposity, reduced skeletal muscle mass, and systemic inflammation. These findings indicate that β-cell dysfunction is a potential therapeutic target in people at risk for developing T2DM and possibly in individuals with maturity-onset diabetes of the young. Although insulin therapy increases body fat in people with established T2DM, this may not be the case for people with maturity-onset diabetes of the young who have β-cell dysfunction but are not insulin resistant. These individuals may derive benefit from insulin therapy as a means of averting weight gain and delaying disease progression.

Funding. M.W. was supported by VIDI grant 91715350 from the Netherlands Organisation for Scientific Research and a Rosalind Franklin Fellowship from the University of Groningen. This research was also supported by a National Health and Medical Research Council of Australia grant (APP1037903) to P.J.B. and K.-A.R. This work was partially funded by National Institutes of Health grant P01 HL087123 (to A.R.T.).

Duality of Interest. No potential conflicts of interest relevant to this article were reported.

Author Contributions. B.J.C. was responsible for the experimental design, performed the experiments and data analysis, and wrote the manuscript. L.H., A.P.C.M., B.M.M., F.T., A.S., L.C.T., S.T., S.S., P.S., and M.P. performed the experiments and data analysis. W.J.R., A.B., M.M., and V.C.W. were responsible for the experimental design. M.W., A.R.T., P.J.B., and K.-A.R. were responsible for the experimental design and wrote the manuscript. K.-A.R. is the guarantor of this work and, as such, has full access to all the data in the study and takes responsibility for the integrity of the data and the accuracy of the data analysis.

Prior Presentation. Parts of this study were presented in abstract form at the 83rd European Atherosclerosis Society Congress, Glasgow, Scotland, 22–25 March 2015; the 17th International Symposium on Atherosclerosis, Amsterdam, the Netherlands, 23–26 May 2015; and the Arteriosclerosis, Thrombosis and Vascular Biology 2014 Scientific Sessions, Toronto, Ontario, Canada, 1–3 May 2014.

References

1. Brooks-Wilson A, Marcil M, Clee SM, et al. Mutations in ABC1 in Tangier disease and familial high-density lipoprotein deficiency. Nat Genet 1999;22:336–345

2. Rust S, Rosier M, Funke H, et al. Tangier disease is caused by mutations in the gene encoding ATP-binding cassette transporter 1. Nat Genet 1999;22:352–355

3. Bodzioch M, Orsó E, Klucken J, et al. The gene encoding ATP-binding cassette transporter 1 is mutated in Tangier disease. Nat Genet 1999;22:347–351

4. Wang N, Lan D, Chen W, Matsuura F, Tall AR. ATP-binding cassette transporters G1 and G4 mediate cellular cholesterol efflux to high-density lipoproteins. Proc Natl Acad Sci U S A 2004;101:9774–9779

5. Out R, Hoekstra M, Habets K, et al. Combined deletion of macrophage ABCA1 and ABCG1 leads to massive lipid accumulation in tissue macrophages and distinct atherosclerosis at relatively low plasma cholesterol levels. Arterioscler Thromb Vasc Biol 2008;28:258–264

6. Kruit JK, Wijesekara N, Westwell-Roper C, et al. Loss of both ABCA1 and ABCG1 results in increased disturbances in islet sterol homeostasis, inflammation, and impaired β-cell function. Diabetes 2012;61:659–664

7. Hao M, Head WS, Gunawardana SC, Hasty AH, Piston DW. Direct effect of cholesterol on insulin secretion: a novel mechanism for pancreatic beta-cell dysfunction. Diabetes 2007;56:2328–2338

8. Vergeer M, Brunham LR, Koetsveld J, et al. Carriers of loss-of-function mutations in ABCA1 display pancreatic beta-cell dysfunction. Diabetes Care 2010;33:869–874

9. Prentki M, Nolan CJ. Islet beta cell failure in type 2 diabetes. J Clin Invest 2006;116:1802–1812

10. Kahn SE. The relative contributions of insulin resistance and beta-cell dysfunction to the pathophysiology of type 2 diabetes. Diabetologia 2003;46: 3–19
11. Vauhkonen I, Niskanen L, Vanninen E, Kainulainen S, Uusitupa M, Laakso M. Defects in insulin secretion and insulin action in non-insulin-dependent diabetes mellitus are inherited. Metabolic studies on offspring of diabetic probands. J Clin Invest 1998;101:86–96
12. O'Rahilly SP, Nugent Z, Rudenski AS, et al. Beta-cell dysfunction, rather than insulin insensitivity, is the primary defect in familial type 2 diabetes. Lancet 1986;2:360–364
13. Pimenta W, Korytkowski M, Mitrakou A, et al. Pancreatic beta-cell dysfunction as the primary genetic lesion in NIDDM. Evidence from studies in normal glucose-tolerant individuals with a first-degree NIDDM relative. JAMA 1995;273: 1855–1861
14. Zonderland ML, Dubbeldam S, Erkelens DW, van Haeften TW. Lower beta-cell secretion in physically active first-degree relatives of type 2 diabetes patients. Metabolism 2000;49:833–838
15. Cali AM, Man CD, Cobelli C, et al. Primary defects in beta-cell function further exacerbated by worsening of insulin resistance mark the development of impaired glucose tolerance in obese adolescents. Diabetes Care 2009;32:456–461
16. Cali' AM, Bonadonna RC, Trombetta M, Weiss R, Caprio S. Metabolic abnormalities underlying the different prediabetic phenotypes in obese adolescents. J Clin Endocrinol Metab 2008;93:1767–1773
17. Weiss R, Caprio S, Trombetta M, Taksali SE, Tamborlane WV, Bonadonna R. Beta-cell function across the spectrum of glucose tolerance in obese youth. Diabetes 2005;54:1735–1743
18. Yeckel CW, Taksali SE, Dziura J, et al. The normal glucose tolerance continuum in obese youth: evidence for impairment in beta-cell function independent of insulin resistance. J Clin Endocrinol Metab 2005;90:747–754
19. Giannini C, Weiss R, Cali A, et al. Evidence for early defects in insulin sensitivity and secretion before the onset of glucose dysregulation in obese youths: a longitudinal study. Diabetes 2012;61:606–614
20. Yokota K, Fukushima M, Takahashi Y, Igaki N, Seino S. Insulin secretion and computed tomography values of the pancreas in the early stage of the development of diabetes. J Diabetes Investig 2012;3:371–376
21. Mitsui R, Fukushima M, Taniguchi A, et al. Insulin secretory capacity and insulin sensitivity in impaired fasting glucose in Japanese. J Diabetes Investig 2012;3:377–383
22. Fukushima M, Usami M, Ikeda M, et al. Insulin secretion and insulin sensitivity at different stages of glucose tolerance: a cross-sectional study of Japanese type 2 diabetes. Metabolism 2004;53:831–835
23. Bogardus C, Tataranni PA. Reduced early insulin secretion in the etiology of type 2 diabetes mellitus in Pima Indians. Diabetes 2002;51(Suppl. 1):S262–S264
24. Koseki M, Matsuyama A, Nakatani K, et al. Impaired insulin secretion in four Tangier disease patients with ABCA1 mutations. J Atheroscler Thromb 2009;16: 292–296
25. Bonora E, Kiechl S, Willeit J, et al.; Bruneck study. Population-based incidence rates and risk factors for type 2 diabetes in white individuals: the Bruneck study. Diabetes 2004;53:1782–1789
26. Pratley RE, Weyer C. The role of impaired early insulin secretion in the pathogenesis of type II diabetes mellitus. Diabetologia 2001;44:929–945
27. Kruit JK, Wijesekara N, Fox JE, et al. Islet cholesterol accumulation due to loss of ABCA1 leads to impaired exocytosis of insulin granules. Diabetes 2011; 60:3186–3196
28. Brunham LR, Kruit JK, Pape TD, et al. Beta-cell ABCA1 influences insulin secretion, glucose homeostasis and response to thiazolidinedione treatment. Nat Med 2007;13:340–347
29. Yvan-Charvet L, Ranalletta M, Wang N, et al. Combined deficiency of ABCA1 and ABCG1 promotes foam cell accumulation and accelerates atherosclerosis in mice. J Clin Invest 2007;117:3900–3908
30. Buchmann J, Meyer C, Neschen S, et al. Ablation of the cholesterol transporter adenosine triphosphate-binding cassette transporter G1 reduces adipose cell size and protects against diet-induced obesity. Endocrinology 2007; 148:1561–1573
31. Westerterp M, Gourion-Arsiquaud S, Murphy AJ, et al. Regulation of hematopoietic stem and progenitor cell mobilization by cholesterol efflux pathways. Cell Stem Cell 2012;11:195–206
32. Carter JD, Dula SB, Corbin KL, Wu R, Nunemaker CS. A practical guide to rodent islet isolation and assessment. Biol Proced Online 2009;11:3–31
33. Kritharides L, Jessup W, Gifford J, Dean RT. A method for defining the stages of low-density lipoprotein oxidation by the separation of cholesterol- and cholesteryl ester-oxidation products using HPLC. Anal Biochem 1993;213: 79–89
34. Stamateris RE, Sharma RB, Hollern DA, Alonso LC. Adaptive β-cell proliferation increases early in high-fat feeding in mice, concurrent with metabolic changes, with induction of islet cyclin D2 expression. Am J Physiol Endocrinol Metab 2013;305:E149–E159
35. Halseth AE, Bracy DP, Wasserman DH. Overexpression of hexokinase II increases insulinand exercise-stimulated muscle glucose uptake in vivo. Am J Physiol 1999;276:E70–E77
36. Scherer T, O'Hare J, Diggs-Andrews K, et al. Brain insulin controls adipose tissue lipolysis and lipogenesis. Cell Metab 2011;13:183–194
37. Karp NA, McCormick PS, Russell MR, Lilley KS. Experimental and statistical considerations to avoid false conclusions in proteomics studies using differential in-gel electrophoresis. Mol Cell Proteomics 2007;6:1354–1364
38. Grant CW, Duclos SK, Moran-Paul CM, et al. Development of standardized insulin treatment protocols for spontaneous rodent models of type 1 diabetes. Comp Med 2012;62:381–390
39. Schneider CA, Rasband WS, Eliceiri KW. NIH Image to ImageJ: 25 years of image analysis. Nat Methods 2012;9:671–675
40. Lu X, Liu J, Hou F, et al. Cholesterol induces pancreatic β cell apoptosis through oxidative stress pathway. Cell Stress Chaperones 2011;16:539–548
41. Takahashi A, Motomura K, Kato T, et al. Transgenic mice overexpressing nuclear SREBP-1c in pancreatic beta-cells. Diabetes 2005;54:492–499
42. Peyot ML, Pepin E, Lamontagne J, et al. Beta-cell failure in diet-induced obese mice stratified according to body weight gain: secretory dysfunction and altered islet lipid metabolism without steatosis or reduced beta-cell mass. Diabetes 2010;59:2178–2187
43. Templeman NM, Clee SM, Johnson JD. Suppression of hyperinsulinaemia in growing female mice provides long-term protection against obesity. Diabetologia 2015;58:2392–2402
44. Templeman NM, Mehran AE, Johnson JD. Hyper-variability in circulating insulin, high fat feeding outcomes, and effects of reducing Ins2 dosage in male Ins1-null mice in a specific pathogen-free facility. PLoS One 2016;11: e0153280
45. Mehran AE, Templeman NM, Brigidi GS, et al. Hyperinsulinemia drives diet-induced obesity independently of brain insulin production. Cell Metab 2012;16: 723–737
46. Yang SY, He XY, Schulz H. Multiple functions of type 10 17beta-hydroxysteroid dehydrogenase. Trends Endocrinol Metab 2005;16:167–175
47. Cooney GJ, Astbury LD, Williams PF, Caterson ID. Insulin response in individual tissues of control and gold thioglucose-obese mice in vivo with [1-14C]2-deoxyglucose. Diabetes 1987;36:152–158
48. Asturias FJ, Chadick JZ, Cheung IK, et al. Structure and molecular organization of mammalian fatty acid synthase. Nat Struct Mol Biol 2005;12: 225–232
49. Teruel T, Hernandez R, Rial E, Martin-Hidalgo A, Lorenzo M. Rosiglitazone up-regulates lipoprotein lipase, hormone-sensitive lipase and uncoupling protein-1, and down-regulates insulin-induced fatty acid synthase gene expression in brown adipocytes of Wistar rats. Diabetologia 2005;48:1180–1188

50. Loftus TM, Jaworsky DE, Frehywot GL, et al. Reduced food intake and body weight in mice treated with fatty acid synthase inhibitors. Science 2000;288:2379–2381
51. Shoelson SE, Herrero L, Naaz A. Obesity, inflammation, and insulin resistance. Gastroenterology 2007;132:2169–2180
52. McTernan PG, Harte AL, Anderson LA, et al. Insulin and rosiglitazone regulation of lipolysis and lipogenesis in human adipose tissue in vitro. Diabetes 2002;51:1493–1498
53. Kosteli A, Sugaru E, Haemmerle G, et al. Weight loss and lipolysis promote a dynamic immune response in murine adipose tissue. J Clin Invest 2010;120:3466–3479
54. Montgomery MK, Hallahan NL, Brown SH, et al. Mouse strain-dependent variation in obesity and glucose homeostasis in response to high-fat feeding. Diabetologia 2013;56:1129–1139
55. Samuel VT, Shulman GI. Mechanisms for insulin resistance: common threads and missing links. Cell 2012;148:852–871